CHEMISTRY OF MATERIALS

Article

pubs.acs.org/cm

Functional Nanosheet Synthons by Covalent Modification of Transition-Metal Dichalcogenides

Stanislav Presolski,[†,‡] Lu Wang,[†] Adeline Huiling Loo,[†] Adriano Ambrosi,[†] Petr Lazar,[§] Václav Ranc,[§] Michal Otyepka,[§] Radek Zboril,[§] Ondřej Tomanec,[§] Juri Ugolotti,[§] Zdeněk Sofer,[∥] and Martin Pumera*[,†]

[†]Division of Chemistry & Biological Chemistry, School of Physical and Mathematical Sciences, Nanyang Technological University, Singapore 637371

[‡]Division of Science, Yale-NUS College, 16 College Avenue West, Singapore 138527

[§]Regional Centre of Advanced Technologies and Materials, Faculty of Science, Department of Physical Chemistry, Palacký University, Olomouc 77146, Czech Republic

[∥]Department of Inorganic Chemistry, University of Chemistry and Technology Prague, Technicka 5, 166 28 Prague 6, Czech Republic

Supporting Information

ABSTRACT: We report on the facile preparation of versatile MoS_2–thiobarbituric acid conjugates, which, in addition to excellent electrochemical behavior, can serve as nanosheet platforms for further functionalization in a multitude of applications. We show that chemically exfoliated MoS_2 was extensively modified with up to 50% surface coverage, while maintaining its metallic character, and that the strategy can be extended to $MoSe_2$, WS_2, and WSe_2. The covalent functionalization endowed the materials not only with good aqueous dispersibility, but also with improved hydrogen evolution reaction (HER) activity, as well as promise in the oxidative detection of DNA nucleobases in solution.

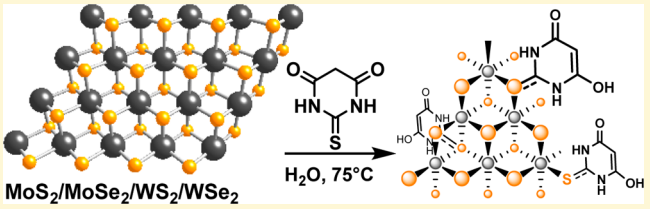

INTRODUCTION

Layered transition metal dichalcogenides (TMDs) have been widely adopted in the preparation of functional two-dimensional (2D) nanomaterials.[1] Their diverse chemical composition and large surface area make them versatile platforms for a myriad applications.[2] Just like graphene they hold the promise to revolutionize the fields of electronics, catalysis, medicine, and more.[3,4] Molybdenum disulfide (MoS_2) and its closely related tungsten and selenium analogues ($MoSe_2$, WS_2, WSe_2) are semiconductors that exist naturally in the hexagonal phase (2H). Mechanical exfoliation of the individual layers or chemical vapor deposition (CVD) bottom-up synthesis produce single-layer materials that have a finite bandgap and are thus suited for semiconducting and optoelectronics applications. Chemical exfoliation, on the other hand, causes large segments of the TMDs to rearrange into the electrically conductive trigonal phase (1T).[5,6] As a result of their catalytically active basal and edge planes and low resistance, the resulting nanosheets are ideal for many electrochemical applications, acting as nonprecious metal electrodes for the hydrogen evolution reaction (HER). While the 1T and 2H classes of TMDs are best suited for different applications, chemical functionalization has until now produced only semiconducting TMDs regardless of the polytype of the starting material.[7] The groups of Chhowalla and Backes have elegantly shown that even if the crystallographic lattice remains 1T, upon functionalization of chemically exfoliated MoS_2 (*ce*MoS_2) with electrophilic reagents the direct bandgap characteristic of the 2H phase is restored.[5,8,7,8] Meanwhile, the more common sulfur vacancy modification strategies have thus far focused almost exclusively on preserving the semiconducting polytype due to its beneficial fluorescence properties in biological applications.[9−11]

In contrast to these efforts, we set out to prepare covalently modified TMDs that maintain their metallic 1T-like properties that are crucial for many important electrocatalytic applications.[12] We employed thiobarbituric acid (TBA) as a nucleophilic thiol reagent to efficiently functionalize the edges and basal planes of chemically exfoliated TMDs while preserving their metallic character. We demonstrate that the high density of coverage endowed the materials with enhanced electrocatalytic properties, in addition to readily accessible hydroxyl handles that can be used for further modification of the nanosheets.

RESULTS AND DISCUSSION

Chemically exfoliated MoS_2, $MoSe_2$, WS_2, and WSe_2 were readily functionalized by stirring overnight with TBA in water

Received: September 30, 2016
Revised: February 8, 2017
Published: February 22, 2017

DOI: 10.1021/acs.chemmater.6b04171
Chem. Mater. 2017, 29, 2066−2073

at 75 °C (Scheme 1). The high surface area and the flat topology of the 2D materials allow for unspecific adsorption of

Scheme 1. Synthesis of Thiobarbituric Acid (TBA)-Modified MoS_2/$MoSe_2$/WS_2/WSe_2 with High Organic Molecule Coverage

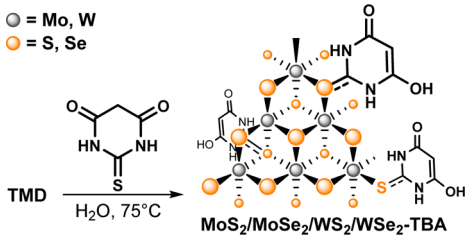

aromatic molecules, so to ensure that only covalently bound TBA remains attached to the TMDs, the materials were subjected to several cycles of rigorous washing (including extensive sonication in acetone−water solution) as described in the Experimental Section. Among many off-the-shelf thiols, thiobarbituric acid was chosen for the TMD modification, because of its reactive sulfur atom, propensity of the molecule for further derivatization, low cost, but also lack of odor.

The resulting TMD−TBA colloidal mixtures were stable for many hours and required centrifugation to separate the solid material from the excess small molecules in solution. When nonaromatic thiols such as cysteine or reduced glutathione were employed instead of TBA, the modified materials were not as well dispersible in water and were thus not pursued further. Despite the increased interest in $MoSe_2$, WS_2, and WSe_2 recently, MoS_2 remains the most widely used and most easily available TMD. Hence, we focused our synthetic and characterization efforts on **MoS_2-TBA**.

Reacting the newly synthesized conjugates with Ellman's reagent established that there were no free sulfhydryl groups in our product, because even after sonication and gentle heating, the test was negative. Therefore, we concluded that the attachment of the thiobarbituric acid derivative is through its nucleophilic sulfur atom, rather than its acidic methylene group. Moreover, once bound, TBA becomes unsusceptible to Knoevenagel condensation with aromatic aldehydes[13,14] but reactive toward activated esters as discussed below. This particular profile of the new nanosheet synthon is indicative of TBA isomerization to yield the structure depicted in Scheme 1, which is one of several conceivable tautomers.[15,16]

The attachment of the TBA molecule to chemically exfoliated MoS_2 was also studied by ab initio calculations within the density functional theory framework. As a model of *ce*MoS_2, we used a single layer of distorted 1T structure of MoS_2 (1T′-MoS_2), because the ideal (CdI_2-type) 1T structure spontaneously relaxed into the distorted phase, in agreement with a recent study.[17] We considered several binding modes of the TBA molecule to MoS_2 (Figure 1A and Figure S1), such as physisorption and attachment through the nucleophilic sulfur atom of all possible tautomers, the most energetically favorable of which are depicted in Figure 1B.

When the TBA molecule is physisorbed, the distance to the surface of MoS_2 is 3 Å, and the bonding arises solely from noncovalent dispersive forces. This finding is corroborated by the fact that the TBA molecule is lying flat on the basal plane (Figure 1A, top left), because such geometry maximizes the dispersive interactions, which add up to an adsorption energy of

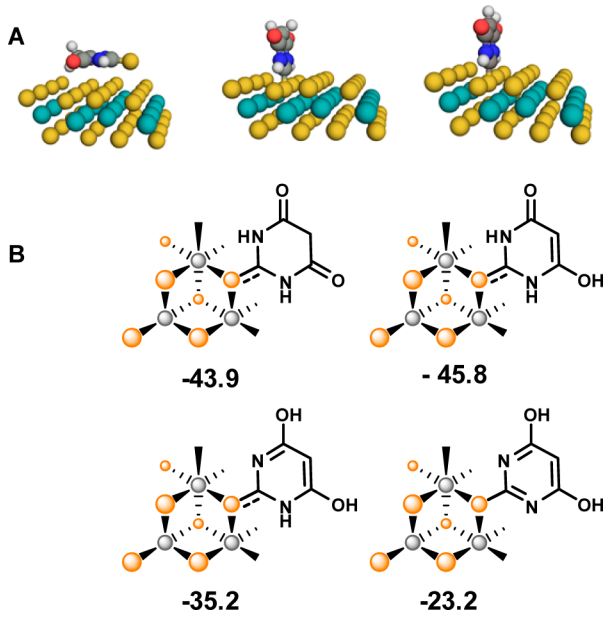

Figure 1. (A) Relaxed geometries of physisorbed (left) and two different covalently bound TBA tautomers (middle and right). (B) Binding energies (kcal/mol) of the most energetically stable **MoS_2-TBA** tautomers.

−18.0 kcal/mol. The covalently bound tautomer, in which the TBA molecule preserves its acidic methylene carbons (Figure 1A, middle), however, has binding energy of −43.9 kcal/mol. The C—S bond length of the bound molecule is 1.76 Å, compared to the 1.64 Å of the isolated molecule, indicating a change from the C═S bond (TBA) to more single-bond character (**MoS_2-TBA**).[18] Tautomerization lowers the energy of the organic−inorganic composite by an additional 1.9 kcal/mol to the monoketo and monoenol forms of TBA (Figure 1B). Thus, the structure depicted in Scheme 1 not only is in excellent agreement with our experimental observations, but is also shown to be the most energetically stable tautomer. Moreover, Raman spectroscopy (Figure 2) confirms the presence of a new C—S covalent bond. The 940 cm^{-1} peak observed in the **MoS_2-TBA** spectrum is in a very good agreement with DFT calculations predicting C—S vibration at 960 cm^{-1} and is not present in unmodified MoS_2 or TBA (Figures 2 and S2). While the E_{2g} and A_{1g} peaks near 400 cm^{-1} are generally attributed to the semiconducting 2H phase,[19] they have been also shown to arise from the partial restacking of the metallic 1T.[20] The electrocatalytic performance of MoS_2 (Figures 5, 8, and 9) strongly suggests the latter, and our theoretical work on 1T′-MoS_2-TBA predicts these two Raman modes as well (Figure S2).

The extent of the TBA coverage was studied by X-ray photoemission spectroscopy (XPS). Samples of the 2D layered MoS_2 were dropcast on platinum foil, which provided the internal standard for our binding energy measurements.[22] No nitrogen peak was observed in the control material (Figure 3, **MoS_2-Φ**), only a small shoulder at higher binding energies (attributed to Mo^{6+} impurity of roughly 14%) in addition to the large Mo $3p_{3/2}$ peak at 393.6 eV.[5] In comparison, the **MoS_2-TBA** spectrum features a strong N 1s signal at 398.6 eV with intensity consistent with approximately 53% TBA modification yield per surface Mo atom. Similar analysis of the S 2p region (165−160 eV) revealed a shoulder centered at 163.4 eV that corresponds to 27% TBA molecules per S atom (see

DOI: 10.1021/acs.chemmater.6b04171
Chem. Mater. 2017, 29, 2066−2073

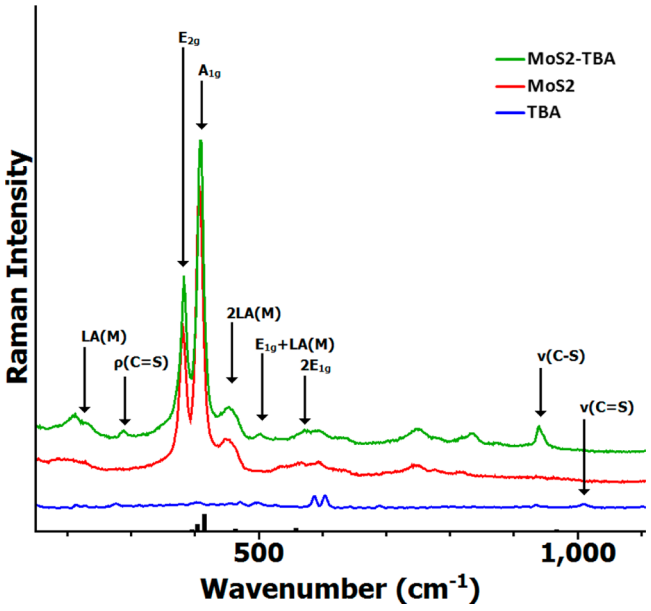

Figure 2. Raman spectra of TBA (blue line), unmodified MoS_2 (red line), and TBA functionalized *ce*MoS_2 (green line) with calculated Raman vibrations and intensities for 1T′-MoS_2-TBA (black bars).[21]

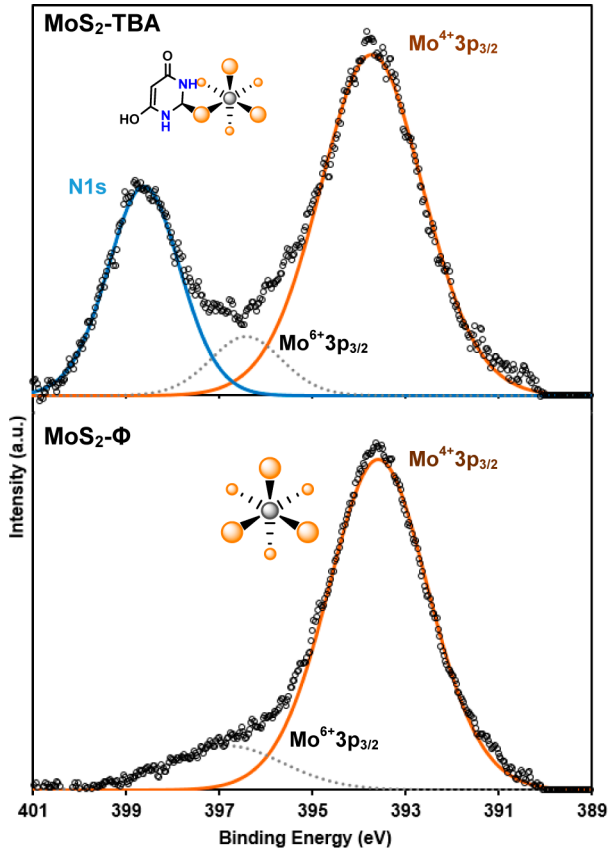

Figure 3. XPS spectra of TBA-functionalized (top) and unmodified (bottom) MoS_2.

Supporting Information, Figures S3 and S4, for high resolution XPS of MoS_2, $MoSe_2$, WS_2, WSe_2, TBA, and their derivatives). Further evidence of the great coverage of *ce*MoS_2 with TBA was provided by HAADF/EDX chemical mapping that showed the homogeneous distribution of nitrogen and oxygen within the sheet (Figure 4 and Figure S5; for EDX of *ce*MoS_2 see Figure S6).

However, the chemical composition determined by XPS and EDX is not representative of the bulk material, especially in the case of *ce*MoS_2, where partial restacking on the nanosheets occurs. Indeed, thermogravimetric analysis revealed that the TBA/Mo molar ratio is 14% (Figure S9a). Further studies of MoS_2, TBA, and **MoS_2-TBA** under nitrogen atmosphere provide significant information on the different thermal behavior of TBA compared to that bound to MoS_2. As expected, the pure MoS_2 structure is thermally stable in the whole studied temperature range. And while TBA starts to decompose at 200 °C, the decomposition temperature of **MoS_2-TBA** is considerably higher at nearly 300 °C. The improved thermal stability of TBA when bound to MoS_2 demonstrates that it is not simply adsorbed onto the TMD nanosheets. In addition, the evolved gas analysis shows that the degradation of **MoS_2-TBA** (Figure S9b) and TBA (Figure S9c) up to 500 °C proceed via considerably different mechanisms. The key released species during the decomposition of **MoS_2-TBA** are SO_2 and SO, while H_2S and HS fragments are not detected. In contrast, the main gases released during the decomposition of TBA are just H_2S/HS without any trace of SO_2/SO.

As a proof-of-concept, **MoS_2-TBA** was treated with acetic anhydride under basic conditions (Scheme 2) to give a material that is better dispersed in acetone than in water, shows different electrochemical behavior (see below), and has been designated **MoS_2-TBA-OAc**. Monocarboxymethylene blue NHS ester was similarly reacted with **MoS_2-TBA**, indicating that other activated esters, anhydrides, as well as electrophiles that can be coupled to acidic alcohols can react with the **MoS_2-TBA** synthon as well.

The strong differential pulse voltammetry (DPV) signal generated by **MoS_2-TBA-MB** shows unequivocally that methylene blue was attached to the surface of the nanosheet synthon (see Figure 5). At the same time, the broad shoulder at slightly higher overpotential to the sharp peak suggests concurrent nonspecific adsorption of the flat, positively charged dye to the 2D negatively charged material. Indeed, when methylene blue without a linker was reacted with *ce*MoS_2, a similarly broad peak was observed. Noteworthy, however, is the lack of any detectable signal when the starting material was **MoS_2-TBA-OAc**. Not only were the alcohol groups protected by acetylation, but the high degree of functionalization appears to block the access of the methylene blue dye to the TMD surface.

The covalent modification of MoS_2 with thiobarbituric acid leads to improved dispersibility of the nanomaterial in water. While exfoliated TMDs can form aqueous suspensions, soon after sonication they start to sediment in the absence of mechanical agitation. Upon standing for several hours most of the material appears to be at the bottom of the vial (Figure 6, top, A). Conversely, **MoS_2-TBA** shows good stability for up to 2 days (Figure 6, top, B). Its acetylated analogue, however, precipitated slightly faster (Figure 6, top, C).

Furthermore, in contact angle measurements (Figure 6, bottom) the negative control material **MoS_2-Φ** does not appear to change its water wettability compared to chemically exfoliated MoS_2. However, the covalent attachment of TBA alters the property of the TMDs dramatically. Acetylation reverts the **MoS_2-TBA** surface to being hydrophobic as can be

DOI: 10.1021/acs.chemmater.6b04171
Chem. Mater. 2017, 29, 2066−2073

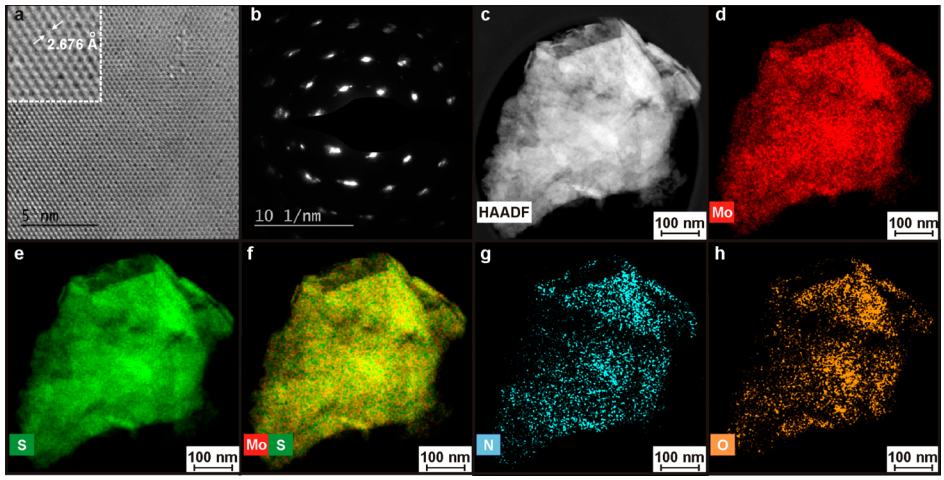

Figure 4. (a) HRTEM image with interlayer spacing corresponding to the (100) plane in the inset; (b) selected area electron diffraction (SAED) pattern; (c) high-angle annular dark-field (HAADF) image; and (d–h) energy dispersive X-ray spectroscopy (EDX) chemical mapping of Mo, S, Mo/S, N, and O within the MoS_2-TBA conjugate.

Scheme 2. Reactions of the MoS_2-TBA Synthon

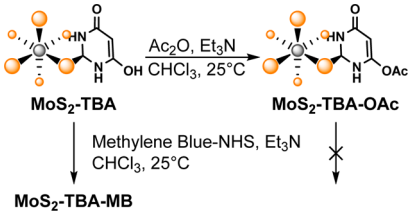

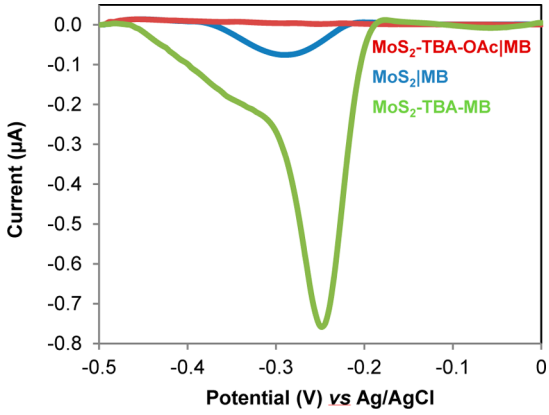

Figure 5. Methylene blue (MB) detection by DPV: virtually nonexistent on MoS_2-TBA-OAc: **MoS_2-TBA-OAc|MB**; only weakly adsorbed on MoS_2: **MoS_2|MB**; and covalently attached on MoS_2-TBA: **MoS_2-TBA-MB**.

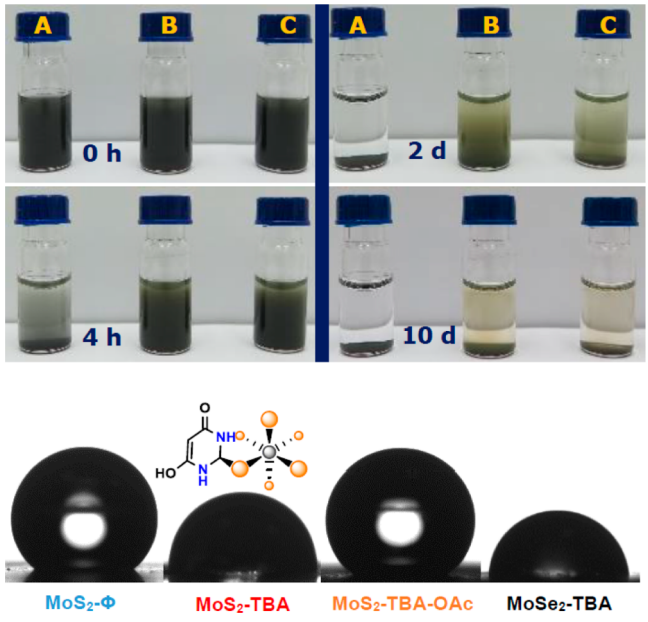

Figure 6. Top: Sedimentation of 1 mg/mL aqueous suspensions of **MoS_2** (A), **MoS_2-TBA** (B), and **MoS_2-TBA-OAc** (C). Bottom: Contact angle measurements (water): **MoS_2-Φ** (140°), **MoS_2-TBA** (98°), **MoS_2-TBA-OAc** (133°), and **$MoSe_2$-TBA** (90°) dropcast as 5 mg/mL acetone suspensions.

expected from the capping of the hydroxyl groups. For additional data on contact angle measurements, see Figure S7.

But despite the de facto removal of the hydroxyl groups **MoS_2-TBA-OAc** remains well dispersed in water due to the presence of other hydrogen bond donors and acceptors, the large amount of small molecules forming a protective sheath that prevents the particles to restack, as well as negative charge on the nanosheets that was presumably unaffected by the acetylation. However, in high ionic strength media such as 100 mM phosphate buffer that can screen the charges, all three materials formed large, insoluble aggregates.

The starting materials for the syntheses outlined in Scheme 1 are *t*-BuLi exfoliated transition metal dichalcogenides. The excess negative charge on the 2D nanosheets[23] causes lattice distortion and a transition from the semiconducting 2H-phase to the metallic 1T′-phase. The 1T/2H polytype ratio determines to a large extent the prevailing properties of the TMD materials, but after the covalent attachment of TBA onto MoS_2, the Mo 4d XPS signature did not change. The two major peaks have shoulders which could be fitted by curves approximately 1 eV higher in energy (Figure 7) indicating that in **MoS_2-TBA** the major polymorph remains the 1T-phase.[5] A certain amount of Mo^{6+} impurity was also present in all spectra,[24] but its relative amount remained approximately the same after chemical functionalization with TBA.

The lower binding energies associated with mixing of the molybdenum orbitals in the octahedral ligand field that we observed by XPS are indicative of material conductive enough

DOI: 10.1021/acs.chemmater.6b04171
Chem. Mater. 2017, 29, 2066–2073

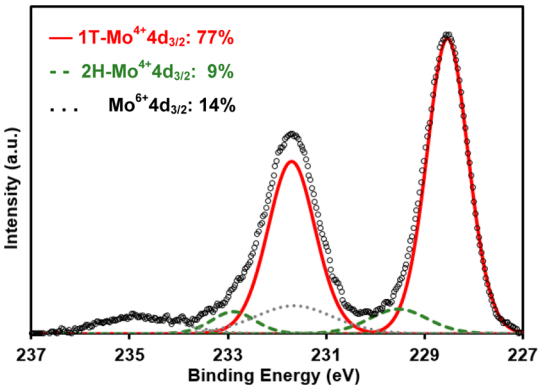

Figure 7. Polytype composition of **MoS_2-TBA**.

to be useful for electrochemical applications. Indeed, the **MoS_2-TBA** showed excellent hydrogen evolution reaction (HER) capabilities in terms of onset potential and Tafel slope (Figures 8A and S8). And unlike the perfectly water-dispersible MoS_2–

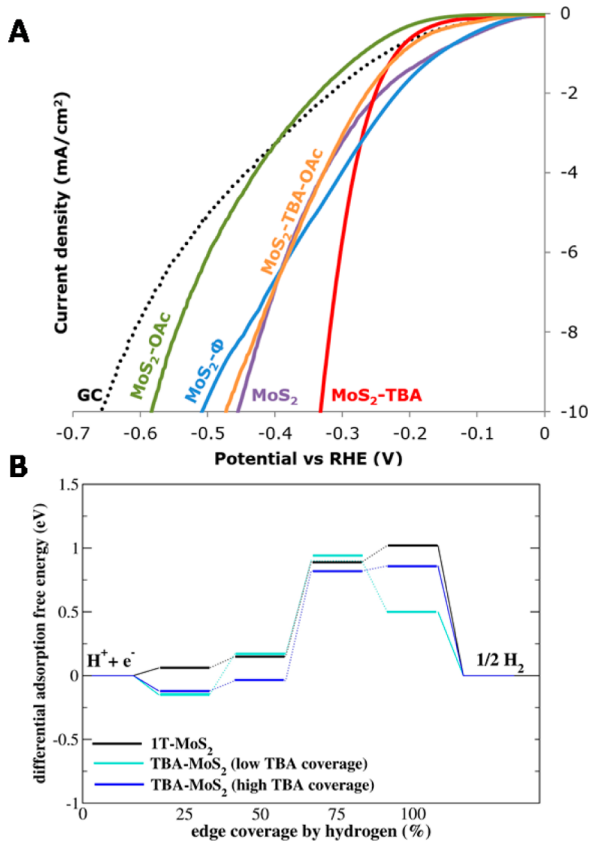

Figure 8. (A) HER linear sweep voltammetry of MoS_2 materials on glassy carbon at pH = 0.[30] (B) Differential adsorption free energy of hydrogen on the edge of 1T-MoS_2 and **MoS_2-TBA** at 6% (low density) and 25% (high density, similar to a value determined by XPS) of TBA molecules with respect to surface S atoms.

PEG material of Huang and Dravid, which had severely diminished HER activity,[25] **MoS_2-TBA** performed much better than its parent MoS_2. We believe the interplay between its inherent 1T-type metallic conductivity,[26] weak surface basicity, and greater wettability make it the best performing catalyst among the tested derivatives. When the hydroxyl groups are acetylated the performance is notably reduced. Treatment of unfunctionalized MoS_2 with acetic anhydride compromised the HER capacity. We suspect that the electrophilic reagent quenched a large number of the negative charges and decreased its conductivity by restoring the bandgap. Similar to the changes observed when methyl iodide was employed,[5] we believe the direct acetylation made our material more 2H-like and thus less electrochemically active.

We were also able to rationalize the enhanced catalytic properties for HER of **MoS_2-TBA** with respect to the parent MoS_2 computationally. The Gibbs free energy of the adsorption of atomic hydrogen (ΔG) is a quantity which can be used to describe the HER activity of the catalyst.[27] The ΔG of an ideal catalyst for HER should be as close to 0 eV as possible.[28] For clean 1T-MoS_2 edge, we obtained ΔG values of 0.06, 0.15, 0.89, and 0.93 eV at 25%, 50%, 75%, and 100% coverage, respectively (defined as the number of hydrogens per number of surface sulfur atoms; black lines Figure 8B), which agree well with recent study by Gao et al.[29] Our calculations predicted that **MoS_2-TBA** is most effective for hydrogen evolution at coverage of up to 50%, because the hydrogen atoms at the edge tend to avoid each other. The **MoS_2-TBA** shows a clear trend of improved catalytic activity at both low and high TBA coverages (light and dark blue lines in Figure 8B),[30] but only when the TBA molecule is covalently attached, which is consistent with the experimental observations.

Having shown that the high density of TBA confers an environment rich in hydrogen bond donors and acceptors, we explored the applicability of **MoS_2-TBA** as a transducing material for the detection of important biomolecules, such as DNA nucleobases. We reasoned that supramolecular interactions between the surface of such material and DNA nucleobases will lead to better electron transfer and hence enhanced electrochemical signals stemming from the oxidation of nucleobases. In order to validate the proposed theory, DEP carbon chips modified with **MoS_2-TBA** and bare DEP carbon chips were utilized for the sensing of DNA nucleobases by differential pulse voltammetry (DPV). As illustrated in Figure 9, by employing **MoS_2-TBA** as the transducing platform, the oxidation peak current of all DNA nucleobases is improved in relation to the bare unmodified platform, with the greatest improvement observed for thymine (T) at 40%. The enhancement in electrochemical signals can be attributed to the formation of H-bonding between the nucleobases and the TBA functionalities on the surface of **MoS_2-TBA**.

In order to further verify that the improvement in electrochemical signals is indeed due to the formation of H-bonding between the TBA functionalities and DNA nucleobases, control experiments were performed using MoS_2 and unfunctionalized disposable carbon electrodes. Figure 9 reveals that, in comparison with **MoS_2-TBA**, when MoS_2 was adopted as the transducing platform, lower electrochemical signals for A, T, and C nucleobases were attained. In particular, the greatest difference in signal intensity is demonstrated by cytosine (C) at 51%. The decrease in electrochemical signals on the MoS_2 platform can be attributed to the lack of H-bonding formation.

It is interesting to note that the T and C nucleobases displayed the greatest enhancement in electrochemical signal on the **MoS_2-TBA** surface. We hypothesize that pyrimidines, being smaller, are capable of engaging more than one TBA molecule through H-bonding and thus are able to bind to the surface better. Nevertheless, more in-depth studies of the nature of this effect are necessary to elucidate the precise mechanism.

DOI: 10.1021/acs.chemmater.6b04171
Chem. Mater. 2017, 29, 2066−2073

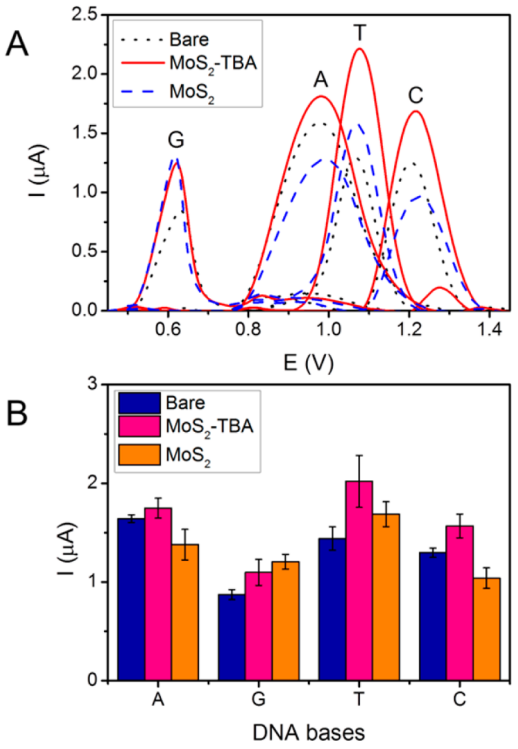

Figure 9. (A) DPV of DNA nucleobases on **MoS_2-TBA** (red solid line), on MoS_2 modified (blue dashed line), and on bare (black dotted line) DEP carbon chips vs Ag/AgCl. (B) Histograms representing the voltammetric response of different DNA nucleobases toward various transducing materials employed. The concentration of nucleobases employed was 1 mM, and all electrochemical measurements were performed in 50 mM PBS buffer solution (pH 7.4) under ambient conditions. Error bars indicate the ±1 standard deviation range obtained from triplicate experiments.

CONCLUSION

In summary, we demonstrated the utility of modifying chemically exfoliated MoS_2 with TBA under aqueous conditions. The high degree of functionalization implies that that the reaction proceeds via a sulfur substitution route, in addition to the more commonly invoked attachment at vacancy sites mechanism. The **MoS_2-TBA** forms stable suspensions in water, but most importantly, the material retains its metallic 1T-type character, which allows it to be used in electrochemical applications such as catalytic HER and nucleobase detection. By virtue of having addressable alcohol groups, the **MoS_2-TBA** can be further modified to endow it with additional functionality, which makes it a true nano building block. Moreover, (thio)-barbiturates offer a tremendous molecular diversity that can be harnessed to attach other chemical handles to MoS_2. Therefore, we expect our facile methodology for creation of diverse TMD synthons to find widespread use.

EXPERIMENTAL SECTION

Materials. Molybdenum disulfide (MoS_2), *tert*-buthyllithium (1.7 M in pentane), and sodium were obtained from Sigma-Aldrich, Czech Republic. Hexane was obtained from Lach-Ner, Czech Republic. Molybdenum diselenide ($MoSe_2$), tungsten disulfide (WS_2), and tungsten diselenide (WSe_2) were obtained from Alfa Aesar, Germany. Argon (99.9999% purity) was obtained from SIAD, Czech Republic.

Synthetic Procedures. *Chemical Exfoliation of TMDCH (MoS_2, WS_2, $MoSe_2$, and WSe_2).* The exfoliated TMDCH was obtained by stirring 3 g of the bulk powder in 20 mL of 1.7 M *t*-butyllithium in pentane for 72 h at 25 °C under an argon atmosphere. Suction filtration was then performed to separate the Li-intercalated compound from the excess intercalant and washed several times with hexane (dried over sodium). The Li-intercalated compound was then placed in water (100 mL) to obtain exfoliation and then centrifuged repeatedly (18000*g*). The obtained material was dried in a vacuum oven at 50 °C for 48 h before further use.

MoS_2-TBA. Chemically exfoliated MoS_2 (25 mg, ~0.15 mmol) and thiobarbituric acid (30 mg, 0.20 mmol) were added to a 4 mL reaction vial with a PTFE-lined cap, suspended in 1 mL of H_2O, sonicated for 5 min at 37 kHz, and heated to 75 °C for 48 h with vigorous stirring. [Shorter reaction times resulted in slightly lower TBA attachment as determined by XPS.] The gray mixture was then allowed to cool, diluted with 3 mL of H_2O, concentrated by centrifugation, and washed 3 times with H_2O, 1 time with a 50/50 mixture of acetone:water, and 3 times with acetone. After each removal of the supernatant, the pellet resuspension and washing was aided by a 5 min sonication. [A less rigorous cleaning procedure resulted in higher apparent yields, but the TBA content evidenced by XPS would decrease with successive washes, indicating some contamination through noncovalent adsorption.] Finally, the product was dried under vacuum overnight to yield 15 mg of dark gray powder.

MoS_2-Φ. Chemically exfoliated MoS_2 was reacted under identical conditions as those for **MoS_2-TBA** but with the omission of thiobarbituric acid.

MoS_2-TBA-OAc. To vacuum-dried **MoS_2-TBA** (5 mg) suspended in anhydrous 0.2 mL of $CHCl_3$ after brief sonication was added one drop (~20 μL) of acetic anhydride and one drop of Et_3N. After 2 h, the suspension was concentrated by centrifugation and extensively washed as described above.

MoS_2-OAc. To chemically exfoliated and vacuum-dried **MoS_2** (5 mg) suspended in 0.2 mL of anhydrous $CHCl_3$ after brief sonication was added one drop (~20 μL) of acetic anhydride and one drop of Et_3N. After 2 h of vigorous stirring at room temperature, the suspension was concentrated by centrifugation, rinsed one time with $CHCl_3$, and then extensively washed as described above.

MoS_2-TBA-MB. **MoS_2-TBA-MB** was prepared similar to **MoS_2-TBA-OAc** but using monocarboxymethylene blue NHS ester (EMPbiotech, see structure below) in the place of Ac_2O.

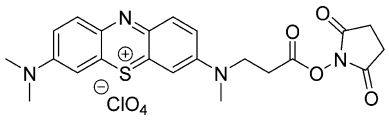

MoS_2-TBA-OAc\|MB. **MoS_2-TBA-OAc\|MB** was prepared similar to **MoS_2-TBA-MB** but using the acetate-capped **MoS_2-TBA-OAc** instead of **MoS_2-TBA**. There was no evidence that covalent attachment or significant adsorption of methylene blue to the nanosheets took place.

MoS_2\|MB. **MoS_2\|MB** was prepared similar to **MoS_2-TBA-MB** but using just the chemically exfoliated **MoS_2** instead of **MoS_2-TBA** and a large excess of methylene blue. The resulting material needed additional washes for the blue color in the mother liquor to appear faint, but some methylene blue remained adsorbed onto the material as evidenced by the DPV measurements.

Analytical Techniques. All differential pulse voltammetry (DPV) measurements were performed on a μAutolab type III electrochemical analyzer (Eco Chemie, The Netherlands) connected to a personal computer and controlled by General Purpose Electrochemical Systems Version 4.9. Electrochemical experiments were conducted with DEP carbon electrodes under ambient conditions. Each DEP carbon electrode comprises a three-electrode system which included a carbon-based working and counter electrode and a Ag/AgCl reference electrode. To modify the working electrode, 3 μL of the material suspension (prepared at 1 mg mL^{-1} concentration in ultrapure water) was dropcast and left to dry. Triplicate measurements were conducted. DPV measurements were performed with the following parameters applied: 1.6 V conditioning potential for 120 s, 50 ms modulation time, 0.5 s interval time, 5 mV step potential, and 25 mV modulation amplitude. DPV data acquired was then treated with a baseline

DOI: 10.1021/acs.chemmater.6b04171
Chem. Mater. 2017, 29, 2066−2073

correction of peak width 0.01 using the GPES software. The HER measurements were conducted in 0.5 M H_2SO_4 aqueous solution, with the sample dropcast as a 5 mg mL^{-1} water suspension on polished glassy carbon electrode, with platinum counter electrode and Ag/AgCl reference electrode.

High-resolution transmission electron microscopy images (HRTEM) were obtained using a HRTEM TITAN 60-300 microscope with an X-FEG type emission gun, operating at 80 kV. This instrument is equipped with a Cs image corrector and a STEM high-angle annular dark-field (HAADF) detector; its point resolution is 0.08 nm in TEM mode. Elemental mappings were obtained by STEM−energy dispersive X-ray spectroscopy (EDS) with an acquisition time of 20 min. For HRTEM analyses, powder samples were dispersed in ethanol and ultrasonicated for 5 min. One drop of the resulting suspension was then placed on a copper grid covered with a holey carbon film and allowed to dry at room temperature.

A combined NTEGRA Spectra system (NT-MDT, Russia) was used to characterize the samples' topography and perform Raman imaging. A 5 μL sample of the as-prepared suspension was deposited on a silicon chip, and the material was characterized immediately after the solvent had evaporated. The surface morphology was characterized in semicontact mode (height and phase) with a VIT_P cantilever (top visual probes, NT-MDT, Russia) having a force constant of 25−95 N/m and resonant frequencies of 200−400 kHz. The scanning rate was 0.5 Hz. Raman mapping experiments were performed using a 532 nm excitation laser with a power of 5 mW applied to the sample.

Thermal gravimetric analysis (TGA) with evolved gas analysis (EGA) was performed using Netzsch STA 449C Jupiter with adapted quadrupole mass spectrometer QMS 403C Aëolos. The measurements were carried out in an open α-Al_2O_3 crucible under nitrogen atmosphere (80 cm^3 min^{-1}). TGA experiments were performed in the temperature range of 40−1000 °C with heating rate of 5 °C min^{-1}. Before each experiment, the crucibles were preheated to 1360 °C and then cooled to room temperature.

■ ASSOCIATED CONTENT

Supporting Information

The Supporting Information is available free of charge on the ACS Publications website at DOI: 10.1021/acs.chemmater.6b04171.

Extensive spectroscopic characterization (PDF)

■ AUTHOR INFORMATION

Corresponding Author

*(M.P.) E-mail: pumera.research@gmail.com.

ORCID

Michal Otyepka: 0000-0002-1066-5677
Radek Zboril: 0000-0002-3147-2196
Martin Pumera: 0000-0001-5846-2951

Notes

The authors declare no competing financial interest.

■ ACKNOWLEDGMENTS

M.P. acknowledges a Tier 2 Grant (MOE2013-T2-1-056; ARC 35/13) from the Ministry of Education, Singapore, and S.P. the Yale-NUS College start-up grant. We are also grateful for the support from the Ministry of Education, Youth and Sports of the Czech Republic (Projects LO1305 and CZ.1.05/2.1.00/19.0377) and the Research Infrastructure NanoEnviCz under Project No. LM2015073, as well as the Czech Science Foundation (GACR No. 16-05167S). This work was supported by the project Advanced Functional Nanorobots (reg. No. CZ.02.1.01/0.0/0.0/15_003/0000444 financed by the EFRR).

■ ABBREVIATIONS

TBA, thiobarbituric acid; TMD, transition metal dichalcogenide; HER, hydrogen evolution reaction; XPS, X-ray photoemission spectroscopy; DPV, differential pulse voltammetry

■ REFERENCES

(1) Chhowalla, M.; Shin, H. S.; Eda, G.; Li, L.-J.; Loh, K. P.; Zhang, H. The chemistry of two-dimensional layered transition metal dichalcogenide nanosheets. *Nat. Chem.* **2013**, *5*, 263−275.

(2) Song, I.; Park, C.; Choi, H. C. Synthesis and properties of molybdenum disulphide: from bulk to atomic layers. *RSC Adv.* **2015**, *5*, 7495−7514.

(3) Service, R. F. Beyond Graphene − The ultrathin form of carbon has inspired other atoms-thick materials that promise even bigger technological payoffs. *Science* **2015**, *348*, 490−492.

(4) Hersam, M. C. The Reemergence of Chemistry for Post-Graphene Two-Dimensional Nanomaterials. *ACS Nano* **2015**, *9*, 4661−4663.

(5) Voiry, D.; Goswami, A.; Kappera, R.; Castro e Silva, C. C.; Kaplan, D.; Fujita, T.; Chen, M.; Asefa, T.; Chhowalla, M. Covalent functionalization of monolayered transition metal dichalcogenides by phase engineering. *Nat. Chem.* **2015**, *7*, 45−49.

(6) Esfahani, D. N.; Leenaerts, O.; Sahin, H.; Partoens, B.; Peeters, F. M. Structural Transitions in Monolayer MoS_2 by Lithium Adsorption. *J. Phys. Chem. C* **2015**, *119*, 10602−10609.

(7) Presolski, S.; Pumera, M. Covalent functionalization of MoS_2. *Mater. Today* **2016**, *19*, 140−145.

(8) Knirsch, K. C.; Berner, N. C.; Nerl, H. C.; Cucinotta, C. S.; Gholamvand, Z.; McEvoy, N.; Wang, Z.; Abramovic, I.; Vecera, P.; Halik, M.; Sanvito, S.; Duesberg, G. S.; Nicolosi, V.; Hauke, F.; Hirsch, A.; Coleman, J. N.; Backes, C. Basal-Plane Functionalization of Chemically Exfoliated Molybdenum Disulfide by Diazonium Salts. *ACS Nano* **2015**, *9*, 6018−6030.

(9) Anbazhagan, R.; Wang, H.-J.; Tsai, H.-C.; Jeng, R.-J. Highly concentrated MoS_2 nanosheets in water achieved by thioglycolic acid as stabilizer and used as biomarkers. *RSC Adv.* **2014**, *4*, 42936−42941.

(10) Liu, T.; Wang, C.; Cui, W.; Gong, H.; Liang, C.; Shi, X.; Li, Z.; Sun, B.; Liu, Z. Combined photothermal and photodynamic therapy delivered by PEGylated MoS_2 nanosheets. *Nanoscale* **2014**, *6*, 11219−11225.

(11) Sim, D. M.; Kim, M.; Yim, S.; Choi, M.-J.; Choi, J.; Yoo, S.; Jung, Y. S. Controlled Doping of Vacancy-Containing Few-Layer MoS_2 via Highly Stable Thiol-Based Molecular Chemisorption. *ACS Nano* **2015**, *9*, 12115−12123.

(12) Chia, X.; Ambrosi, A.; Sedmidubsky, D.; Sofer, Z.; Pumera, M. Precise tuning of charge transfer kinetics and catalytic properties of MoS_2 Materials via Electrochemical Methods. *Chem. - Eur. J.* **2014**, *20*, 17426−17432.

(13) Mageed, A. H.; Al-Ameed, K. A. S. Synthesis and Theoretical Investigation of 5-(4-Dimethylaminobenzylidine) thiobarbituric Acid. *Asian J. Chem.* **2013**, *6*, 2953−2955.

(14) Reaction with ferrocene carboxaldehyde under several different conditions did not change the physical properties of the material. Moreover, neither the characteristic ferrocene peaks nor any iron was detected by CV and XPS, respectively.

(15) Chierotti, M. R.; Gobetto, R. NMR crystallography: the use of dipolar interactions in polymorph and co-crystal investigation. *CrystEngComm* **2013**, *15*, 8599−8612.

(16) Méndez, E.; Cerdá, M. F.; Gancheff, J. S.; Torres, J.; Kremer, C.; Castiglioni, J.; Kieninger, M.; Ventura, O. N. Tautomeric Forms of 2-Thiobarbituric Acid As Studied in the Solid, in Polar Solutions, and on Gold Nanoparticles. *J. Phys. Chem. C* **2007**, *111*, 3369−3383.

(17) Qian, X.; Liu, J.; Fu, L.; Li, J. Quantum spin Hall effect in two-dimensional transition metal dichalcogenides. *Science* **2014**, *346*, 1344−1347.

(18) We have decided to add a dashed line to the C—S bond in the skeletal formula, to avoid confusing the reader in erroneously thinking

DOI: 10.1021/acs.chemmater.6b04171
Chem. Mater. 2017, 29, 2066−2073

that the group between the two nitrogens is CH, when in fact it is a quaternary carbon.
(19) Voiry, D.; Mohite, A. D.; Chhowalla, M. Phase engineered of transition metal dichalcogenides. *Chem. Soc. Rev.* **2015**, *44*, 2702−2712.
(20) Sandoval, S. J.; Yang, D.; Frindt, R. F.; Irwin, J. C. Raman study and lattice dynamics of single molecular layers of MoS_2. *Phys. Rev. B: Condens. Matter Mater. Phys.* **1991**, *44*, 3955−3962.
(21) This plot omits the wavenumber modes below 300 cm^{-1} for clarity. For the full predicted spectrum see Figure S2. Assignment of C═S stretching of TBA is based on Tellez Soto, C. A.; Ramos, J. M.; Costa Junior, A. C.; Vieira, L. S.; Rangel, J. L.; Raniero, L.; Favero, P. P.; Lemma, T.; Ondar, G. F.; Versiane, O.; Martin, A. A. Surface enhancement Raman scattering of tautomeric thiobarbituric acid. Natural bond orbitals and B3LYP/6-311+G (d, p) assignments of the Fourier Infrared and Fourier Raman Spectra. *Spectrochim. Acta, Part A* **2013**, *114*, 475−485.
(22) Spectra are calibrated to Pt^0 $4f_{5/2}$ = 74 eV.
(23) With varying amounts of Li^+ as the counterion.
(24) Song, S. H.; Kim, B. H.; Choe, D.-H.; Kim, J.; Kim, D. C.; Lee, D. J.; Kim, J. M.; Chang, K. J.; Jeon, S. Bandgap Widening of Phase Quilted, 2D MoS_2 by Oxidative Intercalation. *Adv. Mater.* **2015**, *27*, 3152−3158.
(25) Chou, S. S.; De, M.; Kim, J.; Byun, S.; Dykstra, C.; Yu, J.; Huang, J.; Dravid, V. P. Ligand Conjugation of Chemically Exfoliated MoS_2. *J. Am. Chem. Soc.* **2013**, *135*, 4584−4587.
(26) Huang, Y.; Nielsen, R. J.; Goddard, W. A.; Soriaga, M. P. The Reaction Mechanism with Free Energy Barriers for Electrochemical Dihydrogen Evolution on MoS_2. *J. Am. Chem. Soc.* **2015**, *137*, 6692−6698.
(27) Hinnemann, B.; Moses, P. G.; Bonde, J.; Jørgensen, K. P.; Nielsen, J. H.; Horch, S.; Chorkendorff, I.; Nørskov, J. K. Biomimetic hydrogen evolution: MoS_2 nanoparticles as catalyst for hydrogen evolution. *J. Am. Chem. Soc.* **2005**, *127*, 5308−5309.
(28) Zheng, Y.; Jiao, Y.; Jaroniec, M.; Qiao, S. Z. Advancing the Electrochemistry of the Hydrogen-Evolution Reaction through Combining Experiment and Theory. *Angew. Chem., Int. Ed.* **2015**, *54*, 52−65.
(29) Gao, G.; Jiao, Y.; Ma, F.; Jiao, Y.; Waclawik, E.; Du, A. Charge Mediated Semiconducting-to-Metallic Phase Transition in Molybdenum Disulfide Monolayer and Hydrogen Evolution Reaction in New 1T′-Phase. *J. Phys. Chem. C* **2015**, *119*, 13124−13128.
(30) For Tafel slopes, see Supporting Information.

DOI: 10.1021/acs.chemmater.6b04171
Chem. Mater. 2017, 29, 2066−2073